# CHAPTER 5

# MODELING AND ANALYSIS OF SOFC INTEGRATED COMBINED CYCLES WITH THREE DIFFERENT BOTTOMING STEAM TURBINE CYCLES

## 5.1 Introduction

As indicated in Chapter 2, a myriad of potential SOFC–GT hybrid cycle configurations have been proposed and investigated. These hybrid systems can achieve high fuel-to-end-use efficiency with low emissions and also make major contributions to new and secure fossil-fueled energy infrastructure [1]. From literature review in Chapter 2, it was also found that SOFC integrated combined GT–ST cycle is more efficient than the SOFC–GT cycle. The HRSG is the most crucial component in any CC plant (with or without SOFC) where the waste energy of the GT exhaust gases is utilized for generating steam for the bottoming ST (Rankine) cycle. In a conventional boiler, the rate of steam generation depends upon the power load and fuel LHV; accordingly, the necessary amount of fuel is burnt to meet the steam demand. It would also depend upon the exit flue gas temperature, which is usually assumed in most of the cases. This scenario in a HRSG is however different. Arbitrary assumption of the exit gas temperature or the steam generation rate in HRSG may lead to cross temperature situations where the flue gas temperatures at evaporator and economizer exit might become less than the respective steam saturation temperature in the evaporator and economizer water inlet temperature. Under this situation, no steam generation can occur in HRSG. Exhaust gas flow rate, its composition and temperature are very crucial in a HRSG as they greatly influence the steam production. The steam pressure is also another important factor in HRSG with significant effect on steam generation rate and the final exit gas temperature. Some of the recent trends in HRSG design include use of (i) multiple-pressure units for maximum energy recovery, (ii) high temperature superheaters or reheaters in CC plants and (iii) auxiliary firing for efficient steam generation [2].

Besides the above, there are certain other drawbacks of the Rankine cycle for its use in bottoming applications. Steam/water as working fluid in the Rankine cycle is not suitable for high temperature application due to its low critical temperature (375°C). Also due to heat addition at constant vaporization/evaporation temperature, there is always a high temperature difference between the hot flue gas and evaporating water in

the HRSG. Consequently, with high temperature difference between the hot exhaust gas source and the water/steam, the exergy destruction or the irreversibility associated with heat transfer would be more.

In order to reduce the temperature difference between the hot and cold fluid stream, sometime the Rankine cycle is substituted with the Kalina cycle [Fig.5.1] where a mixed working fluid of variable composition is used; a very common is the mixture of water and ammonia. The ammonia has low boiling point and hence it evaporates first reducing its concentration in the mixture. As a result, the boiling temperature of the mixture increases which in turn reduces the temperature difference between the hot exhaust gas and the fluid in the vapor generator causing a rise in the efficiency of the bottoming cycle.

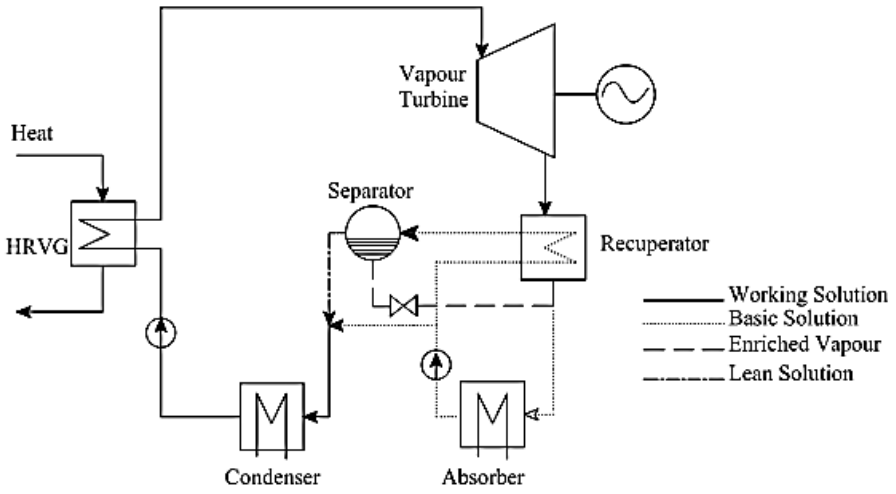


Fig. 5.1: Flow scheme of the Kalina cycle.

Advanced Rankine cycles are also used to maximize energy recovery from hot exhaust gas in HRSG. Some of these cycles are discussed below.

### 5.1.1 Advanced bottoming ST (Rankine) cycles

#### 5.1.1.1 Multi-pressure HRSG

A very recent trend which is used in HRSG design for maximum heat recovery is the use of second (dual) or third pressure level (triple pressure) where steam in the HRSG, instead of producing at a single pressure level is produced at two pressure levels in the dual pressure cycle (high and low) and at three pressure levels (high, intermediate

and low) in the triple pressure cycle. Fig. 5.2 and Fig. 5.3 show three such typical arrangements of dual pressure and triple pressure HRSGs.

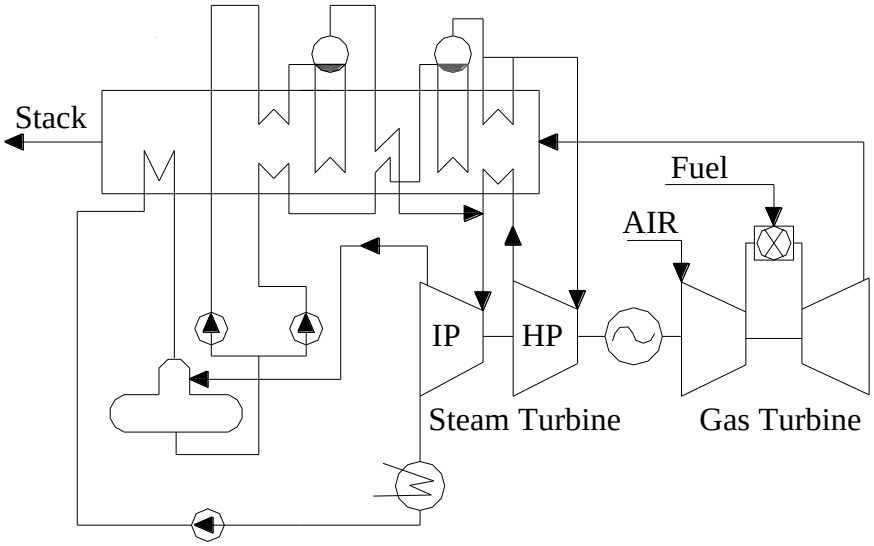


Fig. 5.2: Dual pressure HRSG with reheat

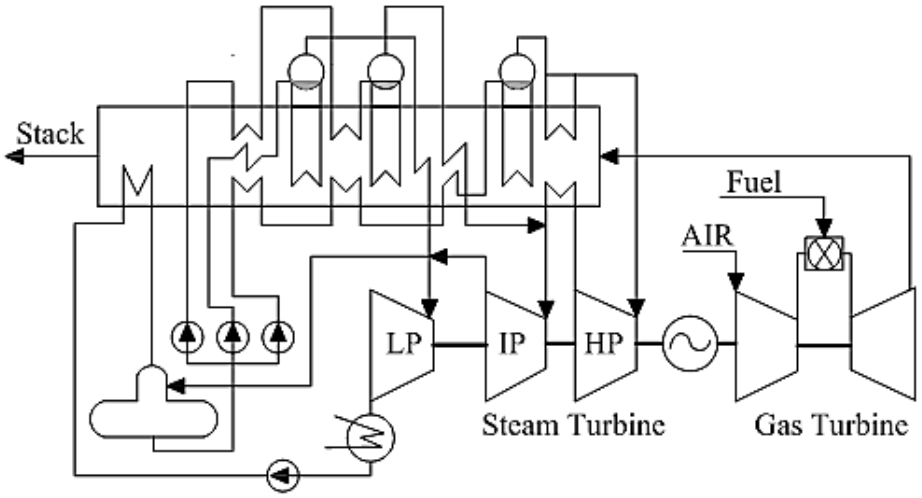


Fig. 5.3: Triple-pressure heat recovery steam generator with reheat [1]

Usually with a single-pressure HRSG, it is possible to generate about 30% of the total plant output in the steam turbine. The power output of the ST cycle can be increased by up to 10% through use of dual-pressure arrangement and a few more percentage of power enhancements is possible through usage of triple-pressure cycle [1, 3].

Efficiency as high as 58.5% was reported for a CC plant that used ABB manufactured GT–26 gas turbine with a triple-pressure reheat HRSG [4]. Jericha *et al.* [5] proposed steam bottoming cycle with five and even more pressure levels in

combination with steam turbo-chargers for obtaining higher efficiency. These are certain arrangements that are practiced for (i) utilizing high temperature exhaust heat with a minimum temperature difference and (ii) avoiding use of mixed working fluid as in the Kalina cycle.

Bottoming ST cycle with multi-pressure HRSG is however not very cost-effective for small scale power generation. There are certain other methods such as (i) water flashing (ii) steam recompression (iii) steam flow splitting which can be used to simplify heat recovery in the HRSG. These are briefly discussed in the following subsections.

### 5.1.1.2 Water flashing

Water flashing is a concept proposed by Dechamps [6] in which vapor at low pressure is produced by extracting pressurized water from the boiler drum and flashing it in a flash tank (Fig. 5.4). With the use of water flashing, efficiency is improved over the single pressure cycle and it is almost comparable with the dual-pressure HRSG scheme.

### 5.1.1.3 Steam recompression

Cheng *et al.* [7, 8] proposed the concept of steam recompression where the steam pressure in the steam drum is raised by means of a compressor (Fig. 5.5). This is useful in a situation where it involves low steam flow rate and it is difficult to split the flow into different pressure levels. Steam recompression bottoming cycle is comparable to the conventional dual-pressure cycle and one notable advantage is that it requires smaller boiler surface area [9].

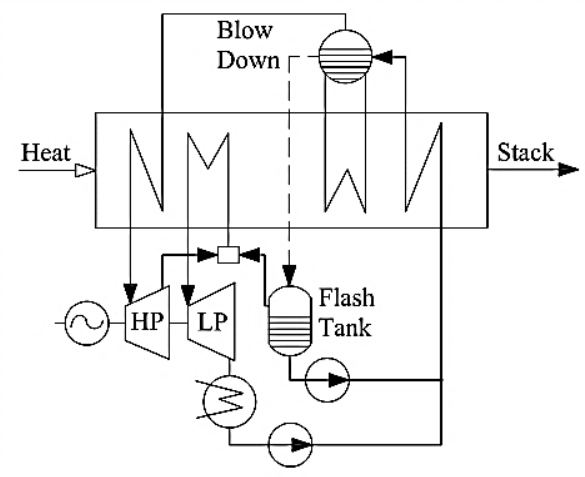


Fig. 5.4: Water flashing [1]

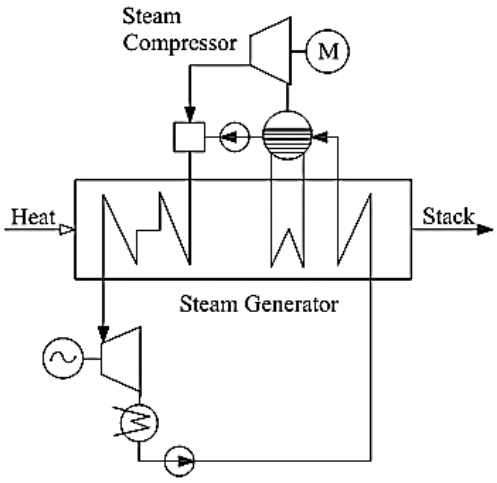


Fig. 5.5: Steam recompression [1]

### 5.1.1.4 Steam flow splitting

The concept of steam flow splitting and recompression is another way that provides operating flexibility to a ST (Rankine) cycle in cogeneration mode under various heat loads [10]. In this system, the excess steam is recompressed to initial pressure by a compressor driven by a back-pressure ST (Fig. 5.6) and a constant flow through the main ST guarantee the full power load while maintaining different heat load conditions. This is certainly better and more efficient than a conventional cogeneration system where varying heat load conditions are accomplished through (i) expansion of excess steam in an expensive low pressure condensing part of the ST which at full heat load would result in significant energy loss, (ii) dumping of excess steam in a dump condenser which by any means can't be a good solution (iii) use of steam injection in a GT which however is possible but would demand a specially designed turbine to work in this mode.

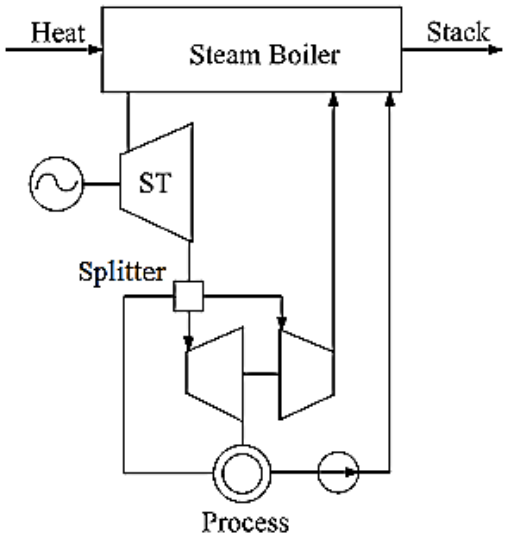


Fig. 5.6: Steam flow splitting in a ST based cogeneration plant

### 5.1.2 Pinch point analysis

The heat transfer in a heat exchanger is governed by the temperature difference between the hot and cold stream. The maximum possible heat transfer is limited by the minimum allowable temperature difference at certain location in the heat exchanger. The point where temperature difference is minimum is called the pinch point and the associated thermodynamic analysis is called as pinch point analysis. Pinch point analysis

provides a systematic methodology for energy saving in heat exchange processes [11, 12].

In a HRSG, the pinch point is the difference between the exhaust gas temperature at evaporator exit and the steam saturation temperature. Pinch point directly affects the steam production and the gas and water/steam temperature profiles. Approach point which is the difference between the saturated steam temperature and water temperature at evaporator inlet is another important HRSG design parameter. Selection of appropriate pinch and approach point is of paramount importance in HRSG design as they affect the size of the heat exchangers (superheater, evaporator, and economizer). No doubt, a low pinch point is desired for increased steam production but in the limit when it is very low, the heat exchanger size would increase infinitely making it costly and unrealistic. The pinch and approach points for unfired HRSGs are usually in the range of 15-30°C [2].

### 5.2 Objective

In this research study, the multi pressure steam boiler concept is adopted in order to reduce temperature difference between hot exhaust gas and water and also as a means of reducing heat transfer irreversibility in the HRSG. A novel SOFC–GT–ST configuration with triple pressure reheat ST cycle is considered to analyze thermodynamically with the help of first law (energy) and second law (exergy) of thermodynamics. Further, the performance of this combined cycle configuration is compared under identical conditions with two other configurations, having dual pressure reheat and single pressure bottoming ST cycles. Pinch principle is applied in modeling HRSG of the three systems. The effect of approach point is however not considered to avoid further complexity in HRSG modeling.

### 5.3 Hybrid SOFC–GT–ST system configuration with triple pressure reheat ST cycle

The SOFC–GT–ST system configuration with triple pressure reheat ST cycle is shown in Fig. 5.7. In this schematic, the GT exhaust is utilized for preheating fuel and air subsequently in the fuel recuperator (FR) and the air recuperator (AR). The exhaust gases leaving the AR is finally utilized to produce steam in the HRSG at three pressure levels viz. high pressure (HP), intermediate pressure (IP) and low pressure (LP). Fuel (methane) and air are compressed in the fuel compressor (FC) and air compressor (AC) respectively. Certain amount of compressed fuel is fed into the SOFC anode via the FR

and the pre-reformer (PR). A PR is used because in SOFC integrated power systems, often partial reforming is done to avoid problems associated with entrance region local sub-cooling, inhomogeneous temperature distributions, thermal stress and anode carbon deposition etc. Therefore, 30% fuel reforming [13] is considered in the PR and this is achieved by mixing steam extracted from the ST at the desired pressure. Remaining 70% fuel is reformed internally within the SOFC utilizing the left over steam from the PR and the heat of the exothermic electrochemical reaction. A part of the compressed fuel is fed directly into the combustor (by-passing the FR, PR and the SOFC) which is burnt along with the SOFC off residual fuels (hydrogen, methane and carbon monoxide) and excess air. The superheated steam produced in the HRSG at HP level is first expanded to IP and then further reheated in the reheater. Steam is again produced in the HRSG IP stage which is fed into the ST together with the original steam at same pressure and temperature for expansion in the ST. Steam is also produced in the HRSG at LP level for expanding it together with the original steam up to the condenser pressure. One open water heater (OWH) is used for the purpose of feed water preheating.

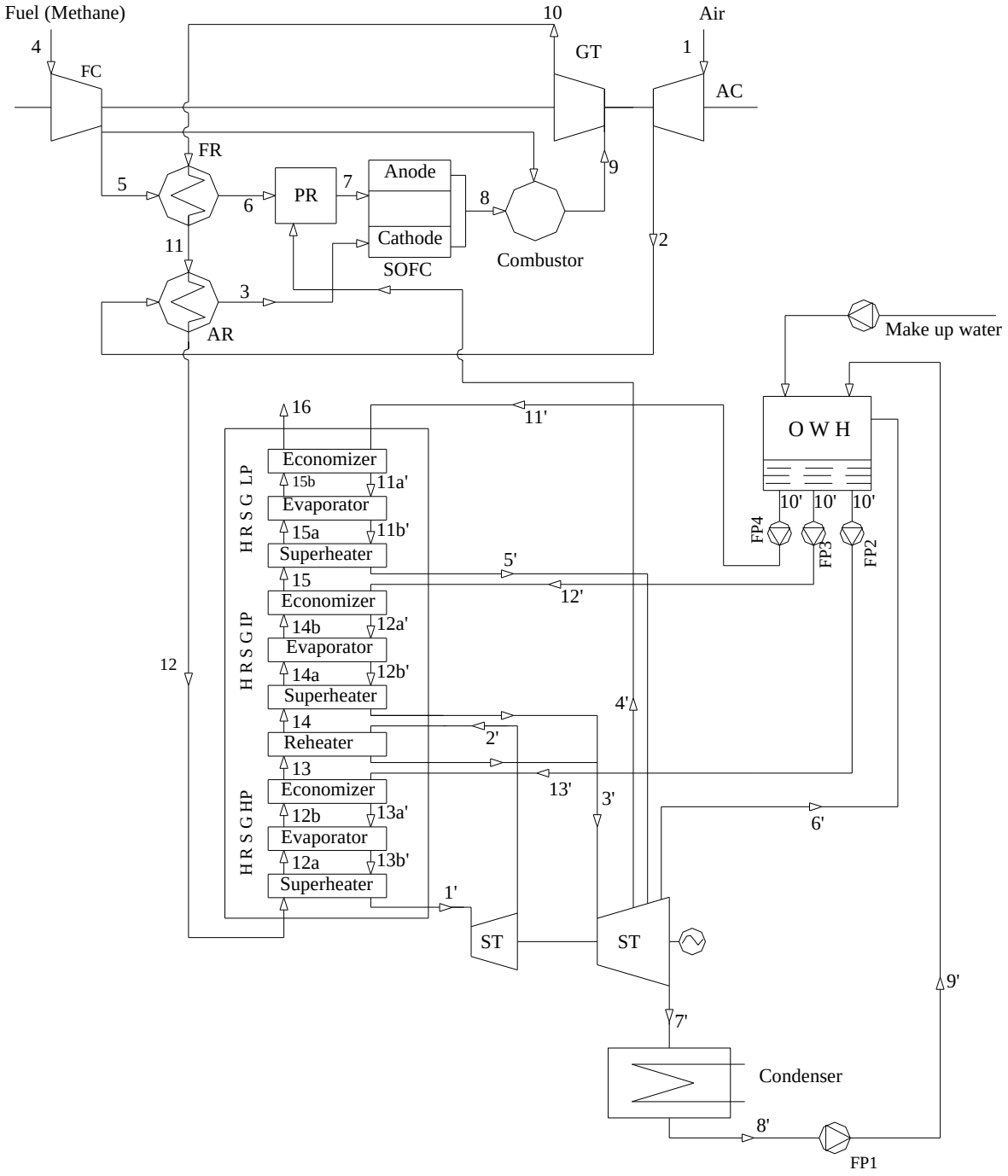


Fig. 5.7: SOFC–GT–ST configuration with triple pressure reheat ST cycle

### 5.4 Dual pressure reheat and single pressure ST cycles

The dual pressure reheat and single pressure ST cycles are also shown separately in Fig. 5.8 and Fig. 5.9. The topping GT cycle is the same in all the three configurations. In the single pressure ST cycle (Fig. 5.9), steam is produced at a single pressure of 40 bar

while in the dual pressure reheat cycle, steam is produced at two pressure levels (200 and 40 bars). The steam produced at 200 bar is first expanded to 40 bar and then further reheated in the reheater. Steam is again generated in the HRSG at 40 bar which enters the ST together with the reheated steam at same temperature for expansion in the ST. The SOFC–GT–ST configuration with single pressure HRSG shown in Fig. 5.9 is different from the one presented in Fig. 3.1 in Chapter 3. In this configuration, we have considered one OWH which was not present in the previous configuration.

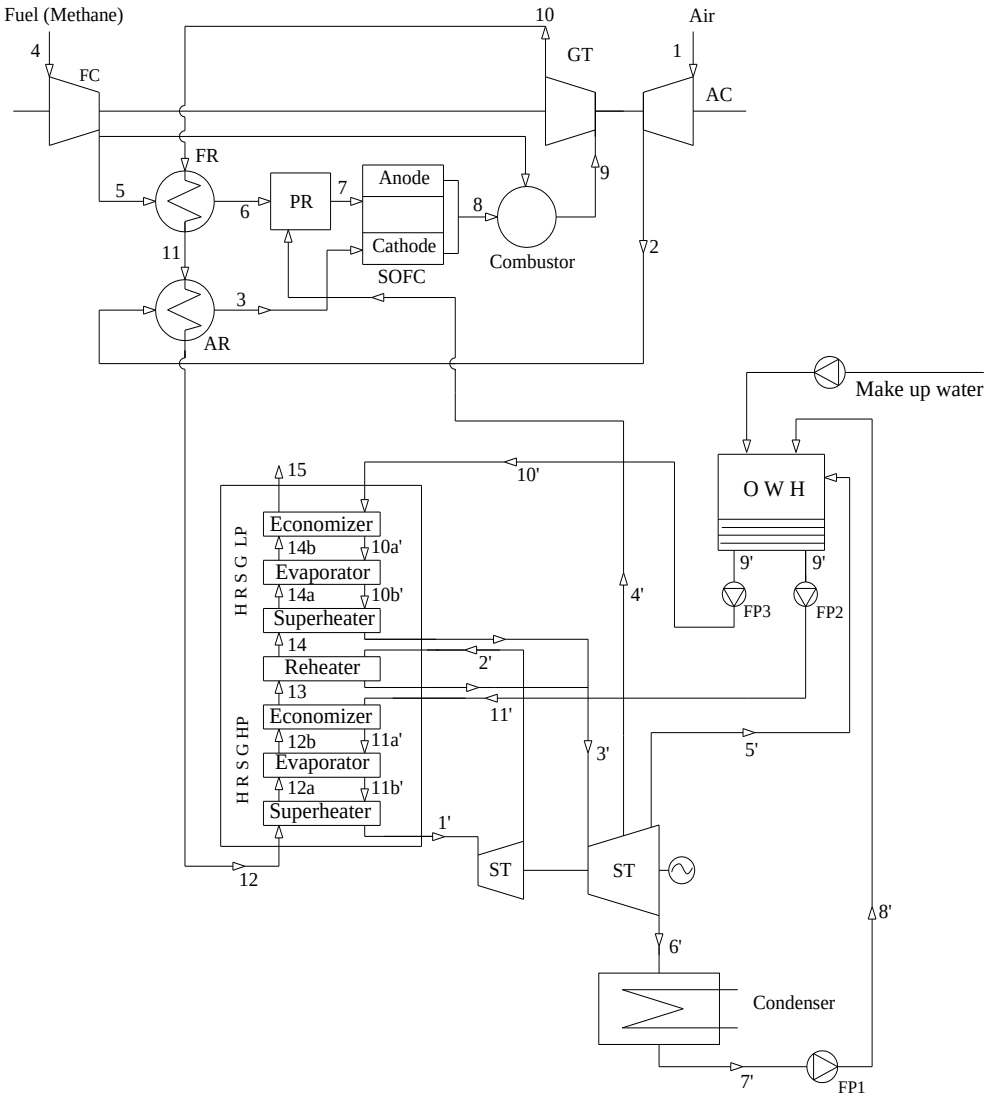


Fig. 5.8: SOFC–GT–ST configurations with dual pressure reheat ST cycle

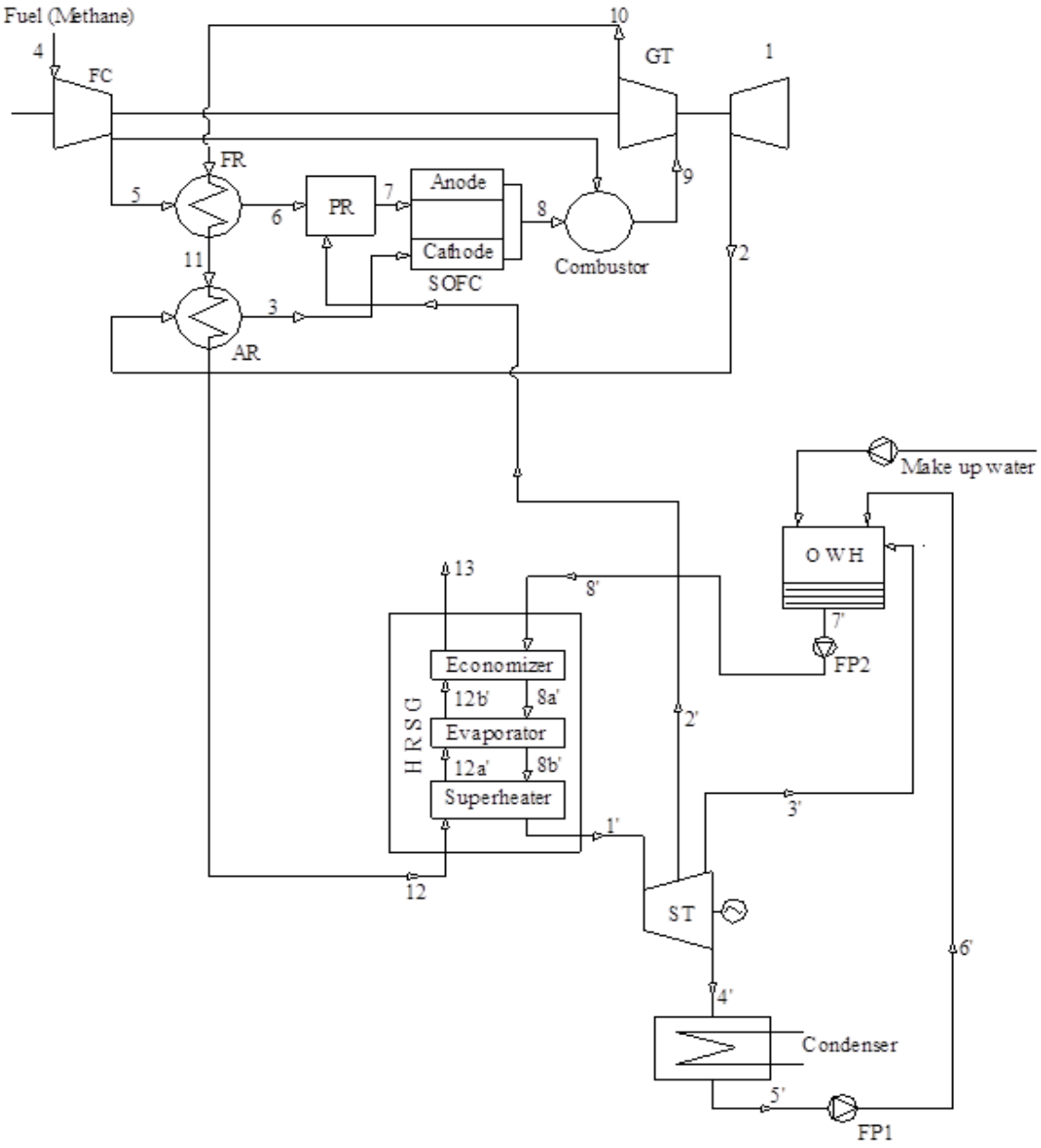


Fig. 5.9: SOFC–GT–ST configurations with single pressure ST cycle

## 5.5 Modeling assumptions

The thermodynamic modeling which is used for simulation of the three SOFC–GT–ST configurations in this chapter is based on the following assumptions: steady state operation; identical cells in the SOFC stack; adiabatic cells with negligible heat loss to the surrounding; ideal gas model for anode, cathode and combustion gases; identical

temperature of anode and cathode exit stream; negligible kinetic and potential energy; standard reference state of 298.15 K and 1.01325 bar; negligible chemical exergy of air and negligible fuel thermo-mechanical exergy. The input parameters assumed for simulation of the SOFC–GT–ST systems with triple pressure reheat, dual pressure reheat and single pressure ST cycle are shown in Table 5.1, Table 5.2 and Table 5.3 respectively. The other input parameters shown for the compressors, SOFC, combustor, GT cycle and the recuperators in Table 5.1 for the system with triple pressure reheat are same for the other two systems with dual pressure reheat and single pressure ST cycles.

## 5.6 Thermodynamic modeling of the topping SOFC–GT cycle

The topping SOFC–GT cycles as shown above in Figs. 5.7-5.9 for the three systems with triple pressure reheat, dual pressure reheat and single pressure ST cycle are the same with that of Fig. 3.1 discussed in Chapter 3. Therefore, the thermodynamic modeling of the topping SOFC–GT cycle which was described in Chapter 3 will also be similar for the topping SOFC–GT cycles in these configurations (Figs. 5.7-5.9). As it was described in detail in Chapter 3, therefore, in this chapter, this is not repeated and instead, only the key points are highlighted.

### 5.6.1 SOFC electrochemical and thermodynamic model

As presented in Chapter 3, the actual voltage of a single fuel cell is the reversible open circuit voltage minus the cell over-potentials (ohmic activation, concentration). The reversible open-circuit voltage of a single fuel cell is calculated using the Nernst equation [27, 15]. Ohmic over-potential is calculated using current density, temperature dependent specific resistivity, coefficients and thickness values of SOFC components [16, 17]. The well-known Butler–Volmer equation is used to calculate the activation over-potential considering a transfer coefficient value of 0.5 [13, 17, 18]. Anode and cathode exchange current density are calculated using equations taken from reference [13]. Concentration over-potential is calculated considering porous electrode structure such as porosity, tortuosity, pore radius and mass transport in the porous electrodes through use of ordinary binary and Knudsen diffusion [13, 19].

Table 5.1: Assumed parameters for SOFC–GT–ST system with triple pressure reheat cycle

| Parameter | Value |
|---|---|
| SOFC | |
| Fuel flow rate | 300 kmol/h |
| Additional fuel flow rate | 100 kmol/h |
| Fuel utilization factor | 0.85 |
| Air flow rate | 45000 kmol/h |
| Oxygen utilization factor | 0.25 |
| Steam to carbon ratio | 2.5 |
| Current density | 0.3 $A/cm^2$ |
| GT cycle | |
| Compressor isentropic efficiency | 85% |
| GT isentropic efficiency | 85% |
| Combustor efficiency | 95% |
| Recuperator (AR and FR) effectiveness | 75% |
| Generator efficiency | 90% |
| Pressure drop | |
| SOFC pressure drop | 4% |
| Recuperator pressure drop (AR and FR) | 4% |
| Combustor pressure drop | 5% |
| HRSG components | 2% for the gas side in all heat exchangers<br>1.5 % in the HP, IP and LP economizers<br>2% in the HP superheater<br>2% in the reheater<br>3% in the IP and LP superheaters |
| ST cycle | |
| HP stage pressure | 200 bar |
| IP stage pressure | 40 bar |
| LP stage pressure | 3.0 bar |
| OWH steam extraction pressure | 1.5 bar |
| Condenser pressure | 0.05 bar |
| ST isentropic efficiency | 80% |
| BFP isentropic efficiency | 80% |
| Generator efficiency | 90% |
| Motor efficiency | 75% |

Source: Reference [14, 22, 23] for pressure drop values

The same SOFC thermodynamic model which was presented in Chapter 3 is used for determining the molar flow rate of the gases taking part in the reforming, shifting and electrochemical reactions. These are determined using molar balance of the reacting species, equilibrium constant values of the reforming and shifting reactions and the fuel utilization factor. Next, the heat of the exothermic reactions (electrochemical and shifting) and the endothermic reforming reaction are determined and then heat balance is applied to calculate the SOFC stack temperature in an iterative manner. The SOFC current is calculated and then the SOFC electric power $\left(Power_{sofc}\right)$is determined by multiplying the cell current with the cell voltage. More details about the SOFC thermodynamic model are available in [20, 16, 13, 21].

Table 5.2: Assumed parameters for SOFC–GT–ST system with dual pressure reheat cycle

| Parameter | Value |
|---|---|
| HRSG components | 2% for the gas side in all heat exchangers<br>1.5 % in the 1st and 2nd stage economizers<br>2% in the 1st stage superheater<br>2% in the reheater<br>3% in the 2nd stage superheater |
| ST cycle | |
| 1st stage pressure | 200 bar |
| 2nd stage pressure | 40 bar |
| OWH steam extraction pressure | 1.5 bar |

Source: Reference [14, 22, 23] for pressure drop values

Table 5.3: Assumed parameters for SOFC–GT–ST system with single pressure ST cycle

| Parameter | Value |
|---|---|
| HRSG components | 2% for the gas side in all heat exchangers<br>1.5 % in the economizer<br>2% in the reheater<br>3% in the superheater |
| ST cycle | |
| Single stage pressure | 40 bar |
| OWH steam extraction pressure | 1.5 bar |

Source: Ref. [14, 22, 23] for pressure drop values

### 5.6.2 SOFC irreversibility calculation

As mentioned previously in Chapter 3, the chemical and the thermo-mechanical exergy of inlet and outlet streams are considered in SOFC irreversibility calculation. Chemical exergy of the component '*i*' at electrode inlet and exit is calculated as given below [13, 17].

$$\dot{E}x_{ch} = \sum_i \dot{n}_i \left[ ex_{ch,i} + \bar{R} T_0 \ln(X_i) \right] \tag{5.1}$$

Similarly, thermo-mechanical exergy:

$$\dot{E}x_{tm} = \sum_i \dot{n}_i \left[ \bar{h}_i(T) - \bar{h}_i(T_0) - T_0 \left( \bar{s}_i^{\,0}(T) - \bar{s}_i^{\,0}(T_0) \right) - \bar{R} \ln \frac{p}{p_0} \right] \tag{5.2}$$

**Total exergy is the sum of the chemical and the thermo-mechanical exergy.**

$$\dot{E}x = \dot{E}x_{ch} + \dot{E}x_{tm} \tag{5.3}$$

Thus SOFC irreversibility: $\dot{I}_{SOFC} = \dot{E}x_3 + \dot{E}x_7 - \dot{E}x_8 - Power_{sofc}$ (5.4)

### 5.6.3 Modeling of other components of the topping GT cycle

The other components of the topping GT cycle are also modeled following the same procedure described in Chapter 3.The composition and temperature of the burnt gas at the combustor exit are determined through energy balance and stoichiometry of the fuel combustion reactions [17]. The combustion gases ($CO_2$, $H_2O$, $O_2$ *and* $N_2$) are

assumed as ideal gas mixture. Molar specific heat and enthalpy of the combustion gases are calculated considering those as temperature dependent. The total mass flow rate, mass based specific heat and characteristic gas constant of the combustion gases are calculated following the procedure outlined in reference [24]. The compressors (AC and FC), the PR and the GT are modeled using methods described in reference [13]. The PR with 30% fuel conversion is modeled using the partial pre-reforming reaction taken from reference [13] and accordingly, the concentrations of species at PR outlet are determined from mass balance. Effectiveness-NTU method is used for modeling AR and FR.

The net power output from the GT plant is calculated as follows.

$$\dot{W}_{net,GT} = \left[\dot{W}_{GT} - \left(\dot{W}_{AC} + \dot{W}_{FC}\right)\right] \times \eta_{gen} \tag{5.5}$$

In the above equation, $\eta_{gen}$ is the generator efficiency. Exergy destruction (irreversibility) occurring in various components is calculated as stated below. Compressor (AC and FC) irreversibility is calculated from the following equation [13]:

$$\dot{I}_C = T_0 \dot{n} \left[ \left( \frac{1-\eta_s}{\eta_s} \right) \ln(CPR) \right] \tag{5.6}$$

PR irreversibility:

$$\dot{I}_{PR} = \dot{E}x_6 + \dot{E}x_2 - \dot{E}x_7 \tag{5.7}$$

The combustor irreversibility is determined from the following exergy balance equation.

$$\dot{I}_{Combustor} = \dot{E}x_5 + \dot{E}x_8 - \dot{E}x_9 \tag{5.8}$$

GT irreversibility:

$$\dot{I}_{GT} = T_0 \dot{n}_g \bar{R} \left[ (1-\eta_{s,GT}) \ln(TER) \right] \tag{5.9}$$

The irreversibility in the recuperators (AR and FR) is calculated using Eq. (5.10).

$\dot{I}_{AR/FR}$ = Decrease in exergy rate of hot stream - Increase in exergy rate of cold stream (5.10)

## 5.7 Thermodynamic modeling of the bottoming ST cycles

The thermodynamic models developed for simulation of (i) triple pressure reheat (ii) dual pressure reheat and (iii) single pressure ST cycles are discussed in the following sub sections. A gas side pressure loss of 2% is considered in every heat exchanger in all three pressure stages of the HRSG including that in the reheater. In the water/steam line also, pressure drops (specified in Tables 5.1-5.3) in the HP, IP and LP economizers and super heaters are considered. Water line pressure losses in the evaporator, OWH and condenser are however neglected.

### 5.7.1 Triple pressure reheat ST cycle

The triple pressure reheat cycle consists of the HRSG, the ST, the condenser, four boiler feed pumps (BFPs), one OWH and a reheater. The HRSG consists of three sections viz. the HP, IP and the LP section. Each section of the HRSG has an economizer (ECO), an evaporator (EVA) and a super-heater (SUP). First, the thermodynamic properties of water and steam at all salient points of the cycle are determined using model equations taken from reference [25]. For calculating steam enthalpy at states $2'$ and $4'-7'$, the turbine isentropic efficiency value is used while water enthalpy at states $9'$ and $11'-13'$ is calculated using pump isentropic efficiency value. After calculating enthalpy values at these specific states, the corresponding temperatures are determined using another set of equations taken from reference [25] and finally the entropy values are calculated.

The temperature of the combustion gas at state 12 is known a priori from the topping GT cycle. A temperature difference of 153°C between the flue gas at state 12b and saturated water at state $13_{a'}$ is selected to calculate the mass flow rate of steam in the HRSG HP stage (200 bar) using Equation, (5.11). The selected temperature difference is sufficient to maintain 15°C-20°C temperature difference between $T_{14}$ and $T_{3'}$ at the entrance of the IP stage superheater. The temperature $T_{3'}$ of superheated steam at reheater and IP stage superheater exit is the same which is assumed 693.15 K. Next, the temperature of exhaust gas at state points 12a is calculated.

$$\dot{m}_{s,HP} = \frac{\dot{m}_g C_{pg,av}\left(T_{12} - T_{12b}\right)}{\left(h_{1'} - h_{13a'}\right)} \tag{5.11}$$

In Eq. (5.11), $C_{pg,av}$ is the mass based average specific heat of the exhaust gas at temperatures $T_{12}$ and $T_{12b}$. The molar specific heat of the combustion gases is calculated using Eq. (5.12) [26] and values of the coefficients $(a_i)$ are taken from reference [27].

$$\frac{C_p}{\overline{R}} = a_1 + a_2 T + a_3 T^2 + a_4 T^3 + a_5 T^4 \tag{5.12}$$

Mass flow rate and mass based specific heat of the combustion gases are determined as follows

$$\dot{m}_g = \sum_i \dot{n}_i M_i \tag{5.13}$$

$$C_{pg} = \sum_i Y_i \frac{C_{p,i}}{M_i} \tag{5.14}$$

In the above equations, $\dot{n}_i$, $Y_i$ and $M_i$ are the rate form molar composition, mass fraction and molecular weight of the gaseous components.

Flue gas temperature at state 13, $(T_{13})$ is initially assumed 1°C lower than $T_{12b}$. Next, $C_{pg,av}$ is determined by averaging its values at $T_{12b}$ and $T_{13}$. Then from energy balance in the economizer of the HP section, the new gas temperature at state 13 is determined iteratively as follows:

$$T_{13,new} = T_{12b} - \frac{\dot{m}_{s,HP}\left(h_{13a'} - h_{13'}\right)}{\dot{m}_g C_{pg,av}} \tag{5.15}$$

In every iteration, $T_{13,new}$ is updated and calculation is repeated until the difference between two successive values is negligibly small.

The steam produced in the HRSG HP stage at 200 bar is first expanded to 40 bar (IP stage) and then reheated in the reheater from $T_{2'}$ to $T_{3'}$. In the reheater, the flue gas temperature decreases from $T_{13}$ to $T_{14}$ and the following iterative procedure is adopted to calculate the exhaust gas temperature at the reheater exit $(T_{14})$.

Flue gas temperature at state 14, $(T_{14})$ is initially assumed 1°C lower than $T_{13}$. Next, $C_{pg,av}$ is determined by averaging its values at $T_{13}$ and $T_{14}$. Then from energy balance in the reheater, the temperature at state 14 is determined in an iterative manner calculating $T_{14,new}$ from Eq. (5.16) and updating its value until the convergence criteria is fulfilled.

$$T_{14,new} = T_{13} - \frac{\dot{m}_{s,HP}\left(h_{3'} - h_{2'}\right)}{\dot{m}_g C_{pg,av}} \tag{5.16}$$

Next, the mass of steam generated in the HRSG IP stage (40 bar) is determined using Eq. (5.17) assuming 40°*C* temperature difference between the flue gas at state 14b and saturated water at state $12_{a'}$. This is also done to maintain a temperature difference in the range of 15°C to 20°C between $T_{15}$ and $T_{5'}$ at entrance of the LP stage superheater.

$$\dot{m}_{s,IP} = \frac{\dot{m}_g C_{pg,av}\left(T_{14} - T_{14b}\right)}{\left(h_{3'} - h_{12a'}\right)} \tag{5.17}$$

$C_{pg,av}$ in the above equation is determined by averaging its values at temperatures $T_{14}$ and $T_{14b}$. Flue gas temperature at state 14a is also simultaneously determined. Gas temperature at state 15 $(T_{15})$ is calculated in an iterative manner using known values of $T_{14b}$, $\dot{m}_{s,IP}$, $h_{12'}$ and $h_{12a'}$.

Following the same procedure, next, the steam generation rate in the HRSG LP stage (3 bar) is calculated using Eq. (5.18). For this calculation however, a temperature difference of 20°C between combustion gas at state 15b and saturated water at state $11'_a$ is assumed.

$$\dot{m}_{s,LP} = \frac{\dot{m}_g C_{pg,av}\left(T_{15} - T_{15b}\right)}{\left(h_{5'} - h_{11_{a'}}\right)} \tag{5.18}$$

$C_{pg,av}$ in Eq. (5.18) refers to its average value at temperatures $T_{15}$ and $T_{15b}$. Simultaneously, the gas temperature at state 15a is determined. And finally, the flue gas temperature at HRSG exit $(T_{16})$ is calculated iteratively using known values of $T_{15b}$,

$\dot{m}_{s,LP}$, $h_{11'}$ and $h_{11a'}$. Thus, the gas temperatures in the HRSG at all states from 12 to 16 are calculated.

The ST power is calculated as follows.

$$\begin{aligned}\dot{W}_{ST} &= \dot{m}_{s,HP}\left(h_{1'}-h_{2'}\right)+\left(\dot{m}_{s,HP}+\dot{m}_{s,IP}\right)\left(h_{3'}-h_{4'}\right)+\left(\dot{m}_{s,HP}+\dot{m}_{s,IP}-\dot{m}_{s,PR}\right)\left(h_{4'}-h_{5'}\right)\\ &+\left(\dot{m}_{s,HP}+\dot{m}_{s,IP}-\dot{m}_{s,PR}+\dot{m}_{s,LP}\right)\left(h_{5'}-h_{6'}\right)+\left(\dot{m}_{s,HP}+\dot{m}_{s,IP}-\dot{m}_{s,PR}+\dot{m}_{s,LP}-\dot{m}_{s,OWH}\right)\left(h_{6'}-h_{7'}\right)\end{aligned} \quad (5.19)$$

where, $\dot{m}_{s,PR}$ is the mass of steam extracted for mixing with fuel prior to its entry to the PR and $\dot{m}_{s,OWH}$ is the mass of steam extracted for feed water heating in the OWH.

Pumping power required in the BFPs is calculated using Eq. (5.20).

$$\begin{aligned}\dot{W}_{BFP} &= \left(\dot{m}_{s,HP}+\dot{m}_{s,IP}+\dot{m}_{s,LP}-\dot{m}_{s,PR}-\dot{m}_{s,OWH}\right)\left(h_{9'}-h_{8'}\right)+\dot{m}_{s,LP}\left(h_{11'}-h_{10'}\right)\\ &+\dot{m}_{s,IP}\left(h_{12'}-h_{10'}\right)+\dot{m}_{s,HP}\left(h_{13'}-h_{10'}\right)+\dot{m}_{s,PR}\left(p_{OWH}-101.325\right)\end{aligned} \quad (5.20)$$

$p_{OWH}$ in the above equation is the OWH pressure in kPa.

The net power output from the ST plant:

$$\dot{W}_{net,ST} = \dot{W}_{ST}\times\eta_{gen}-\frac{\dot{W}_{BFP}}{\eta_{motor}} \quad (5.21)$$

In the above equation, $\eta_{motor}$ is the motor efficiency. Next, irreversible losses in the bottoming ST cycle components are determined. HRSG irreversibility is the sum of exergy destruction in the economizer, evaporator and superheater of all the three pressure sections plus the exergy destruction in the reheater. In a particular component, the irreversibility is calculated by subtracting the increase in exergy of the cold stream (water/steam) from the decrease in exergy of hot exhaust gas stream.

Irreversibility in the other cycle components are determined as follows.

ST irreversibility:

$$\begin{aligned}\dot{I}_{ST} &= \dot{m}_{s,HP}T_0\left(s_{2'}-s_{1'}\right)+\left(\dot{m}_{s,HP}+\dot{m}_{s,IP}\right)T_0\left(s_{4'}-s_{3'}\right)+\left(\dot{m}_{s,HP}+\dot{m}_{s,IP}-\dot{m}_{s,PR}\right)T_0\left(s_{5'}-s_{4'}\right)\\ &+\left(\dot{m}_{s,HP}+\dot{m}_{s,IP}-\dot{m}_{s,PR}+\dot{m}_{s,LP}\right)T_0\left(s_{6'}-s_{5'}\right)+\left(\dot{m}_{s,HP}+\dot{m}_{s,IP}-\dot{m}_{s,PR}+\dot{m}_{s,LP}-\dot{m}_{s,OWH}\right)T_0\left(s_{7'}-h_{6'}\right)\end{aligned} \quad (5.22)$$

Condenser irreversibility:

$$\dot{I}_{COND} = T_0\left[\dot{m}_w C_{pw}\log\left(\frac{t_{w,out}}{t_{w,in}}\right)+\left(\dot{m}_{s,HP}+\dot{m}_{s,IP}+\dot{m}_{s,LP}-\dot{m}_{s,PR}+-\dot{m}_{s,OWH}\right)\left(s_{7'}-s_{8'}\right)\right] \quad (5.23)$$

Irreversibility in the BFPs:

$$\dot{I}_{BFP} = \left(\dot{m}_{s,HP} + \dot{m}_{s,IP} + \dot{m}_{s,LP} - \dot{m}_{s,PR} - \dot{m}_{s,OWH}\right)T_0\left(s_{9'} - s_{8'}\right) + \dot{m}_{s,LP}T_0\left(s_{11'} - s_{10'}\right) + \dot{m}_{s,IP}T_0\left(s_{12'} - s_{10'}\right) + \dot{m}_{s,HP}T_0\left(s_{13'} - s_{10'}\right) + \dot{m}_{s,PR}T_0\left(s_{10'} - s_{17'}\right) \quad (5.24$$

OWH irreversibility:

$$\dot{I}_{OWH} = T_0\left[\left(\dot{m}_{s,HP} + \dot{m}_{s,IP} + \dot{m}_{s,LP} - \dot{m}_{s,PR}\right)s_{10'} - \dot{m}_{s,OWH}s_{6'} - \left(\dot{m}_{s,HP} + \dot{m}_{s,IP} + \dot{m}_{s,LP} - \dot{m}_{s,PR} - \dot{m}_{s,OWH}\right)s_{9'}\right] \quad (5.25)$$

Exergy destructed with the exhaust gases is calculated considering both chemical and thermo-mechanical exergy of exhaust gas stream at the HRSG outlet.

### 5.7.2 Dual pressure reheat ST cycle

In the dual pressure reheat ST cycle (Fig. 5.8), the steam generation rate in the first stage (200 bar) and the gas temperatures at super heater, evaporator and economizer exit are calculated following the same procedure as adopted for the triple pressure cycle. The HP steam produced in the first stage is expanded to 40 bar and further reheated to $T_{3'}$ in the reheater. Again $T_{3'}$ is considered 693.15 K and accordingly the gas temperature at reheater exit is calculated iteratively from energy balance. The exhaust gas is next used for generating superheated steam at 40 bar and $T_{3'}$ in the second stage (40 bar). The steam generation rate in the second stage and gas temperature at state 14a $(T_{14a})$ are determined assuming 20°C temperature difference between $T_{14b}$ and $T_{10a'}$. Finally, the gas temperature at HRSG exit $(T_{15})$ is calculated iteratively using known values of steam mass flow rate, $h_{10'}$, $h_{10a'}$ and $h_{14b}$. The other parameters such as $\dot{W}_{ST}$, $\dot{W}_{BFP}$, $\dot{W}_{net,ST}$ and irreversibility in various components are also calculated adopting similar procedure as described in section 5.7.1.

### 5.7.3 Single pressure ST cycle

In the single pressure ST cycle (Fig. 5.9), steam is produced at a single pressure of 40 bar and no reheating is considered. To calculate steam generation rate, the following equation is used considering 20°C temperature difference between $T_{12b}$ and $T_{8a'}$.

$$\dot{m}_s = \frac{\dot{m}_g C_{pg,av}\left(T_{12} - T_{12b}\right)}{\left(h_{1'} - h_{8a'}\right)} \tag{5.26}$$

$C_{pg,av}$ in the above equation is determined by averaging its value at temperatures $T_{12}$ and $T_{12b}$. Simultaneously, the gas temperature at state 12a and 13 are also determined. The net ST power and component irreversibility are then calculated using known values of enthalpy, entropy and mass flow rate at relevant points of the single pressure ST cycle.

### 5.8 Net power and efficiency of the combined plant

The net power output of the SOFC integrated combined plant:

$$\dot{W}_{net,CC} = Power_{sofc} + \dot{W}_{net,GT} + \dot{W}_{net,ST} \tag{5.27}$$

The energy and exergy efficiency of the combined plant were calculated using the following equations.

$$\eta_I = \frac{\dot{W}_{net,CC}}{\dot{n}_{CH_4} \times LHV} \tag{5.28}$$

$$\eta_{II} = \frac{\dot{W}_{net,CC}}{\dot{n}_{CH_4} \times ex_{CH_4}} \tag{5.29}$$

*LHV* in Eq. (5.28) is the lower heating value and $ex_{CH_4}$ in Eq. (5.29) is the molar specific chemical exergy of fuel. Value of $ex_{CH_4}$ is taken as 830174.37 kJ/kmol.

### 5.9 Performance analysis of SOFC–CC system with triple pressure reheat ST cycle and comparison with dual pressure reheat and single pressure ST cycle

In this section, first, the performance results of the SOFC–GT–ST system with triple pressure reheat ST cycle is presented. After developing the thermodynamic model for the SOFC–GT–ST system with triple pressure reheat ST cycle, next a parametric analysis was done to investigate the effect of CPR on energetic and exergetic performance of the system. This was done also to investigate the effect of CPR on exhaust gas temperature at AR exit (state 12) and STIT $\left(T_{1'}\right)$. The STIT was for this purpose assumed to be 20°C less than the exhaust gas temperature at state 12. This was

assumed to maintain a minimum temperature difference between the two mediums at superheater inlet and also to ensure that STIT in any case does not exceed the allowable limit of maximum 620°C [28]. A temperature difference range of 15–20°C is considered between flue gas and steam at superheater inlet in the high and intermediate pressure stages of the heat recovery steam generator (HRSG). Also, a temperature difference of 20°C is maintained at the pinch point between flue gas and saturated water in the low pressure stage of the HRSG.

### 5.9.1 Effect of CPR on performance SOFC–GT–ST system with triple pressure reheat ST cycle

CPR was varied from 6 to 14 to evaluate its effect on net power and efficiencies (energy and exergy) of the system and also on irreversible losses (irreversibility) occurring in various system components. It was seen that the net power of the system increases with CPR. With increase in CPR, the SOFC power increases due to increase in cell voltage caused by reduction in the cell over potentials at higher operating pressure. The net GT power also increases with CPR due to increase in turbine expansion ratio (TER) and GTIT because the GT power increases at a higher rate than the corresponding increase in the compressor power at higher CPR. The net ST power however reduces slightly with CPR. With increase in CPR, temperature at state 12 decreases and therefore the STIT also decreases causing an overall reduction in the ST power. Low ST power at higher CPR could also be due to reduction in steam generation rate in the HP and LP section of the HRSG as there is an overall reduction in steam mass generated at higher CPR. All these results related to performance variation with CPR are shown in Table 5.4. Moreover, when CPR is increased, the steam required for fuel reforming in the PR is extracted at high pressure and this is also a factor that contributed to low ST power at higher CPR. However, compared to the reduction in ST power, the increase in SOFC and net GT power was more and therefore the net power output was more at higher CPR. Due to increase in net power, the energy and exergy efficiencies also showed an increasing trend with CPR. Further it was seen that the majority of the total power was produced by the SOFC. At CPR 14, the SOFC contributed 59.065 % of the net power and the contribution of the GT and the ST plants to net power was 32.59 % and 8.345 % respectively.

Table 5.4: System performance at various CPR of SOFC–GT–ST system with triple pressure reheat cycle

| | CPR | | | | |
|---|---|---|---|---|---|
| | 6 | 8 | 10 | 12 | 14 |
| SOFC power (MW) | 26.699 | 27.527 | 28.129 | 28.452 | 28.671 |
| Net GT power (MW) | 11.233 | 13.113 | 14.309 | 15.187 | 15.819 |
| Net ST power (MW) | 5.065 | 4.590 | 4.330 | 4.149 | 4.051 |
| Total power (MW) | 42.997 | 45.230 | 46.768 | 47.788 | 48.541 |
| Energy efficiency (%) | 48.252 | 50.757 | 52.482 | 53.627 | 54.473 |
| Exergy efficiency (%) | 46.615 | 49.035 | 50.701 | 51.817 | 52.633 |
| Single cell voltage (V) | 0.550 | 0.568 | 0.581 | 0.588 | 0.593 |
| Stack temperature (K) | 991 | 990 | 990 | 989 | 988 |
| GTIT (K) | 1648.6 | 1649.3 | 1650.9 | 1651.8 | 1652.8 |
| STIT (K) | 886.584 | 874.226 | 869.203 | 866.952 | 867.057 |
| $\dot{m}_{s,HP}$ (kg/s) | 3.654 | 3.319 | 3.180 | 3.116 | 3.119 |
| $\dot{m}_{s,IP}$ (kg/s) | 3.252 | 3.430 | 3.506 | 3.541 | 3.539 |
| $\dot{m}_{s,LP}$ (kg/s) | 0.664 | 0.527 | 0.468 | 0.441 | 0.441 |
| **Irreversibility (MW)** | | | | | |
| HRSG | 3.670 | 3.638 | 3.626 | 3.621 | 3.621 |
| ST | 1.030 | 0.928 | 0.873 | 0.849 | 0.832 |
| COND | 0.125 | 0.115 | 0.111 | 0.109 | 0.109 |
| BPF | 0.022 | 0.021 | 0.020 | 0.020 | 0.020 |
| PR | 4.314 | 4.242 | 4.187 | 4.154 | 4.126 |
| SOFC | 21.942 | 19.861 | 18.383 | 17.380 | 16.627 |
| CC | 8.415 | 8.386 | 8.362 | 8.346 | 8.333 |
| GT | 0.542 | 0.656 | 0.744 | 0.816 | 0.876 |
| FR | 0.477 | 0.496 | 0.500 | 0.497 | 0.490 |
| AR | 0.638 | 0.386 | 0.231 | 0.131 | 0.067 |
| FC | 0.055 | 0.064 | 0.071 | 0.077 | 0.081 |
| AC | 0.621 | 0.720 | 0.798 | 0.861 | 0.914 |
| Exhaust | 1.331 | 1.335 | 1.336 | 1.337 | 1.337 |
| OWH | 0.100 | 0.092 | 0.089 | 0.088 | 0.088 |
| Total | 43.282 | 40.939 | 39.332 | 38.286 | 37.521 |

Exergy destructed (irreversibility) in the system components at various CPR is also shown in Table 5.4. It was seen that the irreversibility in almost all the components decreases with CPR except in the GT, FC and AC. It was also observed that the irreversibility in the FR increases initially during CPR variation which however again decreases at higher CPR. The three components, in which the irreversibility showed an increasing trend with CPR, contribute very little to the total irreversibility; hence the total irreversibility of the system was less at higher CPR. Irreversible losses in the BFP and with the exhaust gas were not affected by CPR variation.

### 5.9.2 Performance comparison of the triple pressure reheat cycle with (i) dual pressure reheat and (ii) single pressure ST cycle

In this study, performance of three SOFC–GT–ST systems with (i) triple pressure reheat (ii) dual pressure reheat and (iii) single pressure ST cycle is compared under some identical operating conditions. Reheating in the single pressure ST cycle was not considered because, steam was produced at 40 bar and therefore, the dryness fraction of steam at ST exit would always be higher than those of the triple and dual pressure reheat cycles. The performance comparison amongst the three cycles at CPR 14 is shown in Table 5.5. It was seen that the system with the single pressure ST cycle produced the highest power amongst the three. Of course, the presented results are specific to the assumptions made, modeling procedure adopted and operating conditions selected for the three bottoming ST cycles. The net power output was the highest for the system with single pressure ST cycle because, although the net ST power was comparatively less, but the SOFC and net GT powers were more compared to those of the other two cycles. The SOFC stack temperature (992 K) was 4°C higher than those of the dual and triple pressure reheat cycles (988 K). This was the reason that GTIT was also relatively high and consequently the SOFC and the GT of this particular combined plant could produce more power. SOFC power was more because the single cell voltage was high. Moreover relatively higher SOFC stack temperature caused reduction in the activation and ohmic over potentials leading to higher cell voltage, although the Nernst potential was slightly less for this cycle than those of the dual and triple pressure reheat ST cycles. In the single pressure ST cycle, the steam from the ST (required for fuel reforming in the PR) was extracted at a higher enthalpy (3349.0 kJ/kg) than those of the dual and triple

pressure reheat cycles (3040.9 kJ/kg). This resulted in comparatively higher SOFC stack temperature.

Usually, SOFC exhibits better performance at temperature above 800°C. High operating temperature demands use of expensive materials for the fuel cell electrodes, electrolyte, interconnects, seals and insulation. Further, SOFC operation at high temperature is highly energy intensive and maintaining a proper balance of plant is a challenging task. For an SOFC system to be cost effective, it must provide reasonable power output at lower operating temperature and therefore, research programs are underway in some countries to develop electrode-supported SOFC using new electrode materials and thin film electrolytes [29, 30, 31, 32]. Electrode-supported SOFCs can be operated at lower temperature in the range from 600°C to 800°C [33] in which the ionic resistance is low due to thinner electrolyte and hence, operating temperature reduces significantly.

Table 5.5: Performance comparison of the SOFC–GT–ST systems with (i) triple pressure reheat (ii) dual pressure reheat and (iii) single pressure ST cycle

| | Triple Pressure reheat cycle | Dual pressure reheat cycle | Single Pressure |
|---|---|---|---|
| SOFC power (MW) | 28.671 | 28.671 | 29.107 |
| Net GT power (MW) | 15.819 | 16.511 | 17.514 |
| Net ST power (MW) | 4.051 | 4.144 | 3.970 |
| Total power (MW) | 48.541 | 49.326 | 50.591 |
| Stack temperature (K) | 988 | 988 | 992 |
| GTIT (K) | 1652.8 | 1652.8 | 1656.0 |
| Single cell voltage (V) | 0.593 | 0.593 | 0.602 |
| Energy efficiency (%) | 54.473 | 55.354 | 56.773 |
| Exergy efficiency (%) | 52.633 | 53.475 | 54.846 |
| $\dot{m}_s$ (kg/s) produced at 200 bar | 3.119 | 2.947 | – |
| $\dot{m}_s$ (kg/s) produced at 40 bar | 3.539 | 4.113 | 7.016 |
| $\dot{m}_s$ (kg/s) produced at 3 bar | 0.441 | – | – |
| Gas temperature at AR exit (°C) | 613.91 | 607.84 | 600.79 |
| Steam quality at ST exit | 0.888 | 0.888 | 0.956 |

The SOFC stack temperature, in this analysis, was however found to be relatively low due to cell cooling by relatively a larger amount of air. Increased air supply to the SOFC affects fuel cell cooling and thus the SOFC stack temperature. Lower operating temperature results in faster start-up, lower thermal stress and longer life of the cell components. The power obtained from the ST of the triple pressure reheat cycle was 4.430 MW; the corresponding power in the dual pressure reheat and single pressure ST cycles were 4.521 MW and 4.262 MW respectively. The total mass of steam generated in the triple pressure reheat cycle was the highest 7.099 kg/s compared to 7.06 kg/s and 7.016 kg/s of the dual and single pressure cycles. In the triple pressure reheat cycle, the BFP pumping power was also comparatively higher which was 378.747 kW against 376.475 kW and 292.203 kW of the dual pressure reheat and single pressure ST cycle. There were four, three and two number of BFPs respectively in the triple pressure reheat, dual pressure reheat and single pressure ST cycle. With the above values of ST and BFP pumping power obtained for the respective cycle, finally the net ST power was found to be the highest for the dual pressure reheat cycle followed by that of the triple pressure reheat and single pressure cycle.

In the single pressure ST cycle, although the enthalpy of superheated steam at ST inlet (state$1'$) was comparatively high, however the steam generation rate was the lowest in this cycle. And the enthalpies of steam at states $1'-4'$ were such that it finally gave a ST power value which was the lowest amongst all. This could be due its lower STIT (580.79°C) compared to 587.84°C of the dual and 593.91°C of the triple pressure reheat cycles. However, since the SOFC power and net GT power were more, therefore, the highest total power was obtained for this cycle. Accordingly, the energy and exergy efficiencies of the SOFC–GT–ST system with single pressure ST cycle were also higher compared to those of the dual and triple pressure reheat cycles. The thermodynamic property data and mass flow rate at various states of the (i) triple pressure reheat (ii) dual pressure reheat and (i) single pressure ST cycle are given in Tables 5.6–5.8.

Table 5.6. Thermodynamic property and mass flow rate at various states of the triple pressure reheat ST cycle

| Triple pressure reheat ST cycle | | | | | |
|---|---|---|---|---|---|
| State | Temperature (°C) | Pressure (bar) | Enthalpy (kJ/kg) | Entropy (kJ/kg K) | Mass flow rate (kg/s) |
| 1′ | 593.91 | 196 | 3525.9 | 6.501 | 3.119 |
| 2′ | 367.29 | 39.592 | 3136.8 | 6.657 | 3.119 |
| 3′ | 420.00 | 38.80 | 3263.3 | 6.856 | 6.658 |
| 4′ | 299.97 | 14 | 3040.9 | 6.955 | 3.750 |
| 5′ | 154.31 | 2.91 | 2771.1 | 7.116 | 0.442 |
| 6′ | 111.35 | 1.5 | 2675.9 | 7.178 | 0.434 |
| 7′ | 32.88 | 0.05 | 2286.1 | 7.496 | 2.910 |
| 8′ | 32.88 | 0.05 | 137.765 | 0.476 | 2.916 |
| 9′ | 32.91 | 1.5 | 137.947 | 0.477 | 2.916 |
| 10′ | 111.36 | 1.5 | 467.081 | 1.433 | 7.100 |
| 11′ | 111.38 | 3.045 | 467.284 | 1.434 | 0.442 |
| 12′ | 111.90 | 40.60 | 472.226 | 1.436 | 3.539 |
| 13′ | 114.17 | 203.00 | 493.596 | 1.447 | 3.119 |

Table 5.7: Thermodynamic property and mass flow rate at various states of the dual pressure reheat ST cycle

| Dual pressure reheat ST cycle | | | | | |
|---|---|---|---|---|---|
| State | Temperature (°C) | Pressure (bar) | Enthalpy (kJ/kg) | Entropy (kJ/kgK) | Mass flow rate (kg/s) |
| 1′ | 587.84 | 196 | 3509.0 | 6.481 | 2.947 |
| 2′ | 362.06 | 39.592 | 3124.0 | 6.637 | 2.947 |
| 3′ | 420.00 | 38.80 | 3263.3 | 6.856 | 7.060 |
| 4′ | 299.97 | 14 | 3040.9 | 6.955 | 3.750 |
| 5′ | 111.35 | 1.5 | 2680.3 | 7.190 | 0.429 |
| 6′ | 32.88 | 0.05 | 2289.9 | 7.509 | 2.881 |
| 7′ | 32.88 | 0.05 | 137.765 | 0.476 | 2.881 |
| 8′ | 32.91 | 1.5 | 137.947 | 0.477 | 2.881 |
| 9′ | 111.36 | 1.5 | 467.081 | 1.433 | 7.060 |
| 10′ | 111.90 | 40.60 | 472.226 | 1.436 | 4.113 |
| 11′ | 114.17 | 203 | 493.596 | 1.448 | 2.947 |

Table 5.8: Thermodynamic property and mass flow rate at various states of the single pressure ST cycle

| Single pressure ST cycle | | | | | |
|---|---|---|---|---|---|
| State | Temperature (°C) | Pressure (bar) | Enthalpy (kJ/kg) | Entropy (kJ/kgK) | Mass flow rate (kg/s) |
| $1'$ | 580.79 | 38.80 | 3631.8 | 7.334 | 7.016 |
| $2'$ | 442.15 | 14 | 3349.0 | 7.435 | 3.750 |
| $3'$ | 210.02 | 1.5 | 2893.1 | 7.686 | 0.390 |
| $4'$ | 32.88 | 0.05 | 2454.0 | 8.045 | 2.876 |
| $5'$ | 32.88 | 0.05 | 137.765 | 0.476 | 2.876 |
| $6'$ | 32.91 | 1.5 | 137.947 | 0.477 | 2.876 |
| $7'$ | 111.36 | 1.5 | 467.081 | 1.433 | 7.016 |
| $8'$ | 111.90 | 40.60 | 472.226 | 1.436 | 7.016 |

The irreversibility occurring in various components of the three systems at CPR 14 is shown in Table 5.9.

Table 5.9: Component irreversibility of the SOFC–GT–ST systems with (i) triple pressure reheat (ii) dual pressure reheat and (iii) single pressure ST cycle

| Irreversibility (MW) | Triple pressure reheat | Dual pressure reheat | Single Pressure |
|---|---|---|---|
| HRSG | 3.621 | 2.044 | 2.137 |
| ST | 0.832 | 0.851 | 0.763 |
| COND | 0.109 | 0.108 | 0.116 |
| BFP | 0.020 | 0.020 | 0.007 |
| PR | 4.126 | 4.115 | 4.011 |
| SOFC | 16.627 | 16.330 | 16.070 |
| CC | 8.333 | 8.333 | 8.319 |
| GT | 0.876 | 0.900 | 0.932 |
| FR | 0.490 | 0.489 | 0.486 |
| AR | 0.067 | 0.074 | 0.081 |
| FC | 0.081 | 0.081 | 0.081 |
| AC | 0.914 | 0.914 | 0.914 |
| Exhaust | 1.337 | 2.568 | 1.900 |
| OWH | 0.088 | 0.087 | 0.093 |
| Total | 37.521 | 36.914 | 35.911 |

It was seen that the SOFC, combustor, PR and the HRSG were the major contributors of irreversibility in all the three systems. Further, it was found that, compared to the triple pressure reheat cycle, the total system irreversibility was comparatively less in the single pressure and dual pressure reheat cycle and it was the minimum in the SOFC–GT–ST system with single pressure ST cycle. It was a direct consequence of the HRSG irreversibility which reduced significantly in the single pressure and dual pressure reheat cycle. HRSG irreversibility was less in the dual pressure cycle because steam was produced in two stages and as such, the 3rd pressure stage (3 bar) was not there and therefore irreversibility occurred in this stage was additional in the triple pressure reheat cycle. Moreover in the dual pressure reheat cycle, the irreversibility of the second stage HRSG components reduced significantly due to 20°C temperature difference selected between $T_{14b}$ and $T_{10a'}$ as compared to 40°C between $T_{14b}$ and $T_{12a'}$ of the triple pressure reheat cycle. But, the 40°C temperature between $T_{14b}$ and $T_{12a'}$ of the triple pressure reheat cycle was otherwise essential in order to maintain 15°C-20°C temperature difference at LP stage superheater inlet. In the single pressure cycle also, a temperature difference of 20°C was selected between $T_{12b}$ and $T_{8a'}$. Further, steam was produced at 40 bar in a single HRSG stage only without reheating, therefore the HRSG irreversibility was found less. However, its value was slightly more compared to that of the dual pressure reheat cycle. The irreversible losses in the combustor, FC, AC, FR of the topping cycle and condenser, OWH and BFP of the bottoming cycle were the same in the systems with dual and triple pressure reheat cycle. Irreversibility was also less in the SOFC and PR of the system with dual pressure reheat ST cycle compared to those of the triple pressure reheat cycle. It was only the ST, GT, AR and particularly the exhaust irreversibility which were more in the dual pressure cycle. The flue gas temperature at HRSG exit of the dual pressure reheat ST cycle was 221.09°C which was significantly higher than the corresponding temperature of the triple pressure reheat (151.7°C). Therefore, the loss of exergy with the flue gas was more in the dual pressure reheat cycle.

In the system with single pressure ST cycle, irreversibility in majority of the system components was less compared to their values in the triple pressure reheat cycle components. The irreversibility in the compressors (FC and AC) of the two systems were the same and only the GT, AR, condenser, OWH and exhaust irreversibility values were slightly higher. It was due to irreversibility reduction primarily in the HRSG and SOFC

that contributed to overall low total irreversibility of the system with single pressure ST cycle in spite of the fact that the exhaust irreversibility at HRSG exit was relatively high. The flue gas temperature at HRSG exit of the single pressure ST cycle was 185.97°C which was higher than the corresponding temperature (151.7°C) of the triple pressure reheat cycle. Therefore, the loss of exergy with the flue gas was more in the single pressure ST cycle compared to that of the triple pressure cycle. Since the flue gas temperature at HRSG exit of the single pressure ST cycle (185.97°C) was less than that of dual pressure reheat cycle (221.09°C), hence exergy loss was comparatively less.

Mansouri *et al.* [23] evaluated exergetic performance of three combined power cycles (dual pressure HRSG, triple pressure HRSG without reheat and triple pressure HRSG with reheat) taking the same gas turbine as topping cycle and fixed GT outlet temperature of 584°C. The HP inlet steam pressures and temperatures were considered same (124 bar and 543°C) in all the bottoming plants. The IP inlet steam pressures and temperatures in the dual pressure and triple pressure without reheat cycles were also taken the same (10.3 bar and 258°C) although the IP and LP inlet pressure conditions were slightly different in the triple pressure reheat (543°C) cycle. They found that the net power and exergy efficiency of the combined cycle were more in the triple pressure cycles and it was the highest for the triple pressure reheat cycle. The exergy losses due to heat transfer in the HRSG and the flue gas exhaust exergy were also less in the triple pressure reheat combined cycle. In the present analysis, however, an opposite scenario was observed i.e. the system with single pressure ST cycle outperforms the systems with dual and triple pressure reheat cycles. This is due to the fact that steam was extracted from the ST for fuel reforming in the PR and this affected the performance of the topping SOFC integrated GT cycle. As a result, the SOFC and net GT powers were more for the system with single pressure ST cycle and this made the difference in the net power output and efficiencies. As opposed to reference [23], the GT outlet temperatures and consequently, the STITs were also different in all the three bottoming cycles due to similar reasons. Moreover, the considered pinch point temperature difference was also responsible for lower HRSG irreversibility in the single pressure and dual pressure reheat ST cycles.

## 5.10 Summary

A thermodynamic model was developed to analyze the energetic and exergetic performance of a SOFC integrated combined cycle power system with triple pressure reheat ST cycle. A parametric study based on CPR variation was performed to evaluate net power, efficiencies (energy and exergy) and irreversibility of the hybrid SOFC–GT–ST system. It was found that the system develops more power output with high efficiency and low irreversibility at higher CPR. The performance comparison amongst the systems with three different bottoming ST cycles showed that the system with single pressure ST cycle performs better compared to those of the dual and triple pressure reheat cycles. The power and efficiency of the system with single pressure ST cycle were the highest amongst all and the total irreversibility was also the minimum for this cycle. The lowest power and efficiency were obtained for the system with triple pressure reheat cycle and it produced the highest total irreversibility. It is obvious that the system with triple pressure reheat cycle would be more complex than the system with single pressure ST cycle. The total cost of this plant including the capital, operating and maintenance cost would be high due to more number of components in it. Therefore, the SOFC–GT–ST system with single pressure ST cycle would be the most appropriate from this point of view. Future studies on thermo-economic optimization maximizing performance or minimizing irreversibility and total cost of the three configurations would provide a better understanding in this regard. Of course, the present findings are useful in providing a thorough understanding about the first and second law performance of the three systems and these are outcome of the selected range (15°C-20°C) of temperature difference at the superheater inlet of all the cycles. The presented results are also crucial due to pinch point temperature difference of 20°C, selected between flue gas and saturated water at the evaporator inlet of (i) HRSG low pressure stage (3 bar) of the triple pressure cycle, (ii) second stage (40 bar) of the dual pressure reheat cycle and (iii) the single stage (40 bar) of the single pressure ST cycle.

**Bibliography**


[1] Korobitsyn, M. A. *New and advanced energy conversion technologies, Analysis of cogeneration, combined and integrated cycles*, PhD thesis, Department of Thermal Engineering, Twente University , Netherlands 1998.

[2] Ganapathy, V. Heat-Recovery Steam Generators: Understand the Basics. *CHEMICAL ENGINEERING PROGRESS*, Technical Report of ABCO Industries, Lunenburg, Canada , August 1996.

[3] Marston, C.H. and Hyre, M. Gas Turbine Bottoming Cycles: Triple-Pressure Steam Versus Kalina. *Journal of Engineering for Gas Turbines and Power*, 117:10-15, 1995.

[4] *Gas Turbine World 1997 Handbook*, Pequot Publishing, Fairfield, CT, USA, 1997.

[5] Jericha, H., Fesharaki, M., and Seyr, A. Multiple Evaporation Steam bottoming Cycle. In *ASME 1997 International Gas Turbine and Aeroengine Congress and Exhibition*, Volume 2 ,Orlando, Florida, USA, June 2–5, 1997.

[6] Dechamps, P.J. A Study of Simplified Combined Cycle Schemes with Water Flashing. In *Proceedings of the Florence World Energy Research Symposium (FLOWERS'94)*, Florence, Italy, July 6–8, 1994.

[7] Cheng, D.Y. Pressure-Staged Heat Exchanger. U.S. Patent 4,072,182, 1978a.

[8] Cheng, D.Y. Regenerative Parallel Compound Dual-Fluid Cycle Heat Engine.U.S. Patent 4,128,994, 1978b.

[9] Grimaldi, C.N. and Desideri, U. Performance Analysis of Combined Cycles: Steam60 cogeneration, combined and integrated cyclesn Recompression vs Conventional Bottoming Cycles. In *ASME 1997 International Gas Turbine and Aeroengine Congress and Exhibition*, Volume 4, Hague, Netherlands, June 13–16, 1994.

[10] Lievense, C. and Hirs, G.G. Stoomflowsplitsing Middels Stoomcompressie (Steam Flow Splitting through Steam Compression). Internal Report, Comprimo Consulting Services, Amsterdam, Netherlands, 1986.

[11] March, L. Introduction to Pinch Technology. Northwich, Cheshire CW9 7UZ, England, 1998.

[12] Rokni, M. Introduction to Pinch Technology. Division of Energy Section , Technical University of Denmark, Kgs. Lyngby, Denmark ,2016.

[13] Bavarsad, P. G. Energy and exergy analysis of internal reforming solid oxide fuel cell–gas turbine hybrid system. *International Journal of Hydrogen Energy*, 32: 4591 – 4599, 2007.

[14] Haseli, Y., Dincer, I., and Naterer, G.F. Thermodynamic modeling of a gas turbine cycle combined with a solid oxide fuel cell. *International Journal of hydrogen energy*, 33:5811-5822, 2008.

[15] Park, S.K. and Kim, T.S. Comparison between pressurized design and ambient pressure design of hybrid solid oxide fuel cell–gas turbine systems. *Journal of Power Sources*, 163:490–499, 2006.

[16] Chan, S.H., Ho, H.K., and Tian, Y. Modelling a simple hybrid SOFC and gas turbine plant. *Journal of power sources*, 109:111-120, 2002.

[17] Calise, F., Palombo, A., and Vanoli, L. Design and partial load exergy analysis of hybrid SOFC–GT power plant, *Journal of Power Sources*, 158:225–244, 2006.

[18] Gorla, R.S.R., Pai, S.S., and Rusick, J.J. Probabilistic analysis of solid oxide fuel cell based hybrid gas turbine system. Technical Report No. NASA/TM—2003-211995, E-13666, NAS 1.15:211995, GT–2003–38046, NASA Glenn Research Center, Cleveland, OH, United States, 2003.

[19] Chan, S.H., Khor, K.A., and Xia, Z.T. A complete polarization model of a solid oxide fuel cell and its sensitivity to the change of cell component thickness. *Journal of Power Sources, 93:130*–140, 2001.

[20] Massardo, A. F. and Lubelli, F. Internal Reforming Solid Oxide Fuel Cell–Gas Turbine Combined Cycles (IRSOFC–GT): Part A—Cell Model and Cycle Thermodynamic Analysis. *Journal of Engineering for Gas Turbines and Power*, 122: 27-35, 2000.

[21] Chan, S.H., Low, C.F., and Ding, O.L. Energy and exergy analysis of simple solid oxide- fuel cell systems. *Journal of power sources*, 103:188-200, 2002.

[22] Arsalis, A. Thermoeconomic Modeling and Parametric Study of Hybrid Solid Oxide Fuel Cell – Gas Turbine – Steam Turbine Power Plants Ranging from 1.5 MWe to 10 MWe. *Journal of power sources*, 181: 313-326, 2008.

[23] Mansouri, M.T., Ahmadi, P., Kaviri, A. G., Jaafar, M. N. M. Exergetic and economic evaluation of the effect of HRSG configurations on the performance of combined cycle power plants. *Energy Conversion and Management*, 58: 47–58, 2012.

[24] Gogol, T.K. A combined cycle plant with air and fuel recuperator for captive power application, Part 1: Performance analysis and comparison with non-recuperated and gas turbine cycle with only air recuperator. *Energy Conversion and Management*, 79: 771–777, 2014

[25] Wagner, W. , Cooper, J. R., Dittmann, A. , Kijima ,J., Kretzschmar, H.J. , Kruse,A., Mares, R., Oguchi, K. , Sato, H. , Stocker, I. ,Sifner, O., Takaishi, Y., Tanishita, I. ,Trubenbach, J. , and Willkommen, T. The IAPWS Industrial Formulation 1997 for the thermodynamic properties of water and steam. *Journal of Engg. for Gas Turbine and Power*, 122 :150-181,2000.

[26] Talukdar, K. and Gogoi, T.K. Exergy analysis of a combined vapor power cycle and boiler flue gas driven double effect water–LiBr absorption refrigeration system. *Energy Conversion and Management*, 108:468–47, 2016.

[27] Moran, M.J. and Shapiro, H.N. *Fundamental of Engineering Thermodynamics*. John Wiley & Sons, Singapore,4th edition, 2005.

[28] Cengel, Y. A. and Boles, M.A. *Thermodynamics: An Engineering Approach*. Tata McGraw-Hill, 5th edition, 2006.

[29] Stambouli, A. B. and Traversa, E. Solid oxide fuel cells (SOFCs): a review of an environmentally clean and efficient source of energy. *Renewable and Sustainable Energy Reviews*, 6: 433–455, 2002.

[30] Shao, Z. and Haile, S. M. A high-performance cathode for the next generation of solid oxide fuel cells. *Nature*, 431(7005):170-173, September 2004.

[31] Wei, B., Lu, Z., Huang, X., Liu, Z. Miao, J., Li, N., and Su, W. Ba0.5Sr0.5Zn0.2Fe0.8O3_d Perovskite Oxide as a Novel Cathode for Intermediate-Temperature Solid-Oxide Fuel Cells. *Journal of Am. Ceram. Soc*., 90 (10): 3364–3366, 2007.

[32] Atkinson, A. , Barnett, S., Gorte, R. J., Irvine, J. T. S., McEvoy, A. J., Mogensen, M. ,Singhal, S. C.,Vohs, *Journal of Advanced anodes for high-temperature fuel cells, Nature Materials*, 3: 17–27,2004.

[33] Zhang, S., Bi, L., Zhang, L., Yang, C., Wang, H., Liu, W. Fabrication of cathode supported solid oxide fuel cell by multi-layer tape casting and co-firing method. *International Journal of Hydrogen Energy*, 34:7789-7794, 2009.